Preprint Title Silver nanoparticles nucleated in NaOH treated halloysite: a potential antimicrobial material.

Authors Yuri B. Matos, Rodrigo S. Romanus, Mattheus Torquato, Edgar H. de Souza, Rodrigo L. Villanova, Marlene Soares and Emilson R. Viana

Publication Date 15 März 2021

Article Type Full Research Paper

Supporting Information File 1 supp.fig.A.png; 466.3 KB

ORCID® iDs Rodrigo S. Romanus - https://orcid.org/0000-0003-1139-5776; Rodrigo L. Villanova - https://orcid.org/0000-0002-1515-6935; Marlene Soares - https://orcid.org/0000-0003-4066-3338; Emilson R. Viana - https://orcid.org/0000-0002-1883-3508

Silver nanoparticles nucleated in NaOH treated halloysite: a potential antimicrobial material

Y. B. Matos[1], R. S. Romanus[2], M. Torquato[3], E. H. de Souza[4], R. L. Villanova[5], M. Soares[6] and E. R. Viana*[7]

Address: [1]Departamento Acadêmico de Física, Universidade Tecnológica Federal do Paraná - UTFPR - Curitiba, Brazil; [2]Departamento Acadêmico de engenharia Mecânica, Universidade Tecnológica Federal do Paraná - UTFPR - Curitiba, Brazil; [3]Secção de Engenharia e Ciência dos Materiais, Instituto Militar de Engenharia - IME - Rio de Janeiro, Brazil; [4]Departamento Acadêmico de Física, Universidade Tecnológica Federal do Paraná - UTFPR - Curitiba, Brazil; [5]Departamento Acadêmico de engenharia Mecânica, Universidade Tecnológica Federal do Paraná - UTFPR - Curitiba, Brazil; [6]Departamento Acadêmico de Química e Biologia, Universidade Tecnológica Federal do Paraná - UTFPR - Curitiba, Brazil and [7]Departamento Acadêmico de Física, Universidade Tecnológica Federal do Paraná - UTFPR - Curitiba, Brazil

Email: E. R. Viana - emilsonjunior@professores.utfpr.edu.br

* Corresponding author

Abstract

Despite all recent advances in medical treatments, infectious diseases remain dangerous. This scenario has led to intense scientific research on materials with antimicrobial properties. Silver nanoparticles (Ag-NPs) are a well established solution in this area. The present work studied the nucleation of silver in halloysite substrates (HNT) modified by a NaOH chemical treatment. The resulting stabilized Ag-NPs were characterized by X-ray diffraction (XRD), transmission electron microscopy (TEM) and energy dispersive x-ray spectroscopy (EDS). The nucleation was characterized by thermogravimetric analysis (TGA) and differential scanning calorimetry (DSC). Ag-NPs antimicrobial properties were investigated against *E. coli* and *S. aureus*. The potential of Ag-NPs

for industrial application was tested by dispersing them into low density polyethylene (LDPE). The importance of the chemical affinity between matrix and additive was tested coating Ag-NPs with dodecanethiol, a non-polar surfactant. The resulting composites were characterized by scanning electron microscopy (SEM) and in terms of surface antimicrobial activity. The results demonstrate that Ag-NPs synthesized in this work are indeed antimicrobial, and that it is possible to imbue a polymeric matrix with the Ag-NPs antimicrobial properties.

Keywords

antimicrobial activity; silver nanoparticles; halloysite; DIO coating; nanocomposites;

Introduction

Deaths from bacterial infections have been significantly reduced with the emergence of antibiotics, but some bacterial diseases still remain amongst the most dangerous to human life. In addition, as antibiotics become more popular, bacteria are evolving to become resistant — a phenomenon known as “antimicrobial resistance”, and listed by the World Health Organization as one of the top ten threats to public health[1]. Research on antimicrobial nanomaterials is one of the most promising antibiotic free alternative for many applications; among them metallic nanoparticles, which could be potent inorganic antimicrobial agents in due to ion-releasing properties and the capability to rupturing the cellular membrane and disrupting internal cellular components, such as the DNA [2-6].

Silver nanoparticles (Ag-NPs), in particular, are specially prominent for their antimicrobial properties, being one of the most studied inorganic antimicrobial agents [7-9]. Early studies sugest that Ag-NPs displays strong growth-inhibitory properties against common microorganisms, and that they may be used as an alternative way to overcome bacterial resistance to antibiotics [10,11]. However, large scale industrial usage of Ag-NPs is still limited, because most synthesis techniques used in lab are unsuitable to commercial use — the main issues being high procedural complexity and elevated costs, which jeopardize scalability efforts fundamental to industrial mass-production of Ag-NPs.

Amongst the most scalable synthesis routes for Ag-NPs, some techniques stand out by using stabilizers — such as PVP [12] or PEG [13] capping agents — to ensure that silver nucleates and stabilizes into nanosized particles, instead of dissolving back into Ag^+ ions or growing up to microscale. Some routes stabilize Ag-NPs by nucleating silver onto clay substrates [14,15], such as kaolinite [16-18], montmorillonite [17-20] and halloysite nanotubes [21-23]. The advantages are, for instance, preventing particle agglomeration, improving dispersability into polymeric matrices, keeping good biocompatibility with the human body, immobilizing Ag-NPs into substrate, which provides better interaction with bacteria and is a more eco-friendly way to obtain a antimicrobial agent.

Halloysite (HNT) is a natural clay, consisting of an aluminosilicate sheet which folds over itself in virtue of the internal stress inherent to the material's crystalline structure, forming nanotubes [24]. As shown in figure 1, it folds with a silicate phase facing outwards (Si-O), and an aluminol phase facing inwards (Al-OH). Since HNT's internal and external surfaces have different chemical constitutions, they display different chemical affinities as well. Silver nucleation, for example, is favoured on the aluminol surface, due the high affinity between Ag^+ ions and hydroxyls (OH^-) [25]; and there is even evidences suggesting that silver nucleation in HNTs external surface tends to occur in crystalline defects, where aluminol is exposed [22]. Synthesizing Ag-NPs supported by HNT has the advantage of improving stability, thus enhancing antimicrobial properties of the material [21-23,26,27].

In this work we treated the HNT surface with NaOH to improve Ag-NP nucleation into the clay substrate. The resulting nanocomposite was evaluated in terms of chemical composition, morphology and antimicrobial properties, while the nucleation process was characterized in terms of thermal behaviour and structural changes. We also investigated the Ag-NPs potential for industrial application by dispersing them into low density polyethylene (LDPE), providing a way to evaluate chemical compatibility between matrix and additive by testing a dodecanethiol (DIO) coating to improve Ag-NPs dispersion into LDPE. The resulting composites were then evaluated in terms of surface antimicrobial activity.

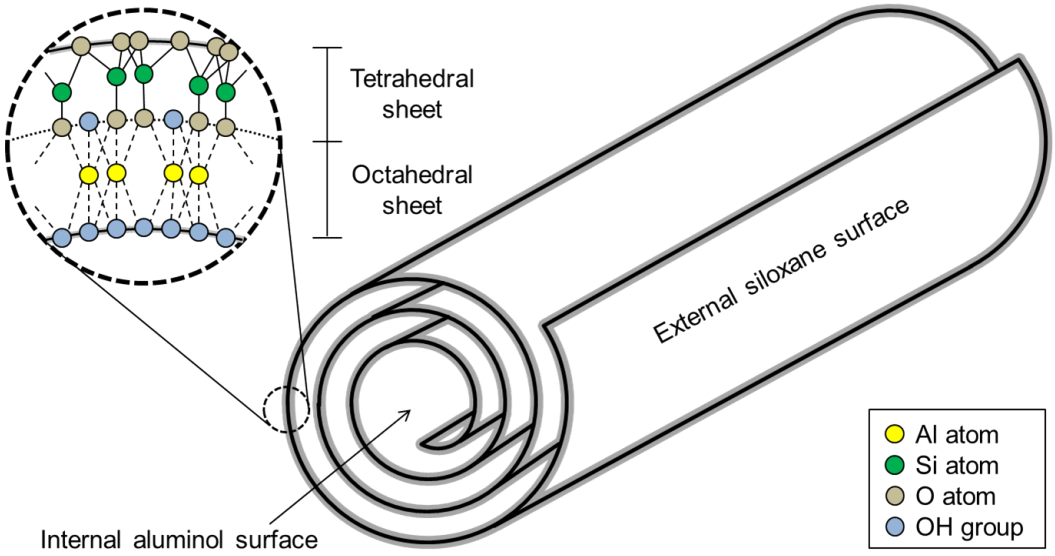

Figure 1: Crystal structure of halloysite particles.

Materials and Methods

Halloysite (>99%), silver nitrate ($AgNO_{3(s)}$, >99%) and dodecanethiol were obtained from Sigma Aldrich; sodium hydroxide ($NaOH_{(s)}$, >99%) was purchased from Alpha Quimica; low Density Polyethilene (LDPE) from Braskem.

Transmission electron microscopy (TEM) was performed in a Jeol JEM-1400 plus (480 keV), energy dispersive x-ray spectroscopy (EDS) and Scanning Electron Microscopy (SEM) in a Zeiss EVO MA15, and thermogravimetric analysis (TGA) and differential scanning calorimetry (DSC) in a simultaneous thermal analyzer Netzsch STA 449 F3. X-ray Diffraction (XRD) measurements were carried out using a Shimadzu diffractometer, model XRD-7000, with Cu K-α radiation (λ = 0.154 nm).

Substrate preparation

To prepare the substrates for silver nucleation, halloysite was treated in a NaOH(aq) bath. Three HNT suspensions were prepared sonicating 100 g of HNT powder into 400 mL of deionized water (DI), for 20 min, at 20 kHz. One suspension, labelled HNT-0, was not subjected to the NaOH(aq) treatment, and was used as a control sample. The two remaining suspensions received 200 g of

NaOH, which were stirred until complete dissolution, followed by resting periods of four and eight days – resulting in the samples HNT-4 and HNT-8. After the resting periods, the three suspensions were filtered and extensively washed with deionized water to remove residual NaOH and then dried naturally. To characterize the prepared substrates, samples HNT-0, HNT-4 and HNT-8 were subjected to TEM, while sample HNT-8 was also subjected to XRD (XRD was also performed for HNT-0 and HNT-4 but omitted from this report because it did not show any significant difference from HNT-8).

Silver nanoparticle synthesis

To synthesize silver nanoparticles, 10 g of HNT (from the three samples previously prepared: HNT-0, HNT-4 and HNT-8) were dispersed in 20 mL of $AgNO_3$ solution (3 molar) and left to rest for one day to load the silver nitrate into the clay structure. Then the samples were filtered, dried at 80 °C for 3 h, and heated to 500 °C for 15 min, to reduce $AgNO_3$ into metallic silver. They were then labelled Ag/HNT-0, Ag/HNT-4 and Ag/HNT-8 (according to the NaOH treatment), and characterized by TEM and EDS. The Ag/HNT-8 was also characterized by XRD.

Ag-NPs nucleation analysis

In order to study the nucleation of silver nanoparticles, 1 g of Ag/HNT-8 were submited to TGA and DSC analysis, from room temperature up to 600°C, at constant heating of 20 °C/min.
In order to observe the phases identified in the DSC/TGA measurements, four 10 g samples of HNT-8 were loaded with $AgNO_3$ using the process described in the section "silver nanoparticle synthesis", heated up to 65 °C, 105 °C, 230 °C and 505 °C and them TEM images were obtained to correlate morphological changes occurring during the synthesis with the thermodynamic data from DSC/TGA analysis.
Finally, another 10 g of HNT-8 were loaded with $AgNO_3$ and heated up to 700 °C, with visual inspections being performed at 40 °C, 100 °C, 120 °C, 200 °C, 350 °C, 500 °C and 700 °C, to evaluate the colour changes during the heating process.

Minimal Inhibitory Concentration test (MIC)

The bactericide effect of Ag/HNT-8 and Ag/HNT-0 were evaluated by a Minimal Inhibitory Concentration (MIC) test. The first step was to obtain pure strains of the bacteria chosen for the test: *Escherichia coli* (ATCC 25922) and *Staphylococcus aureus* (ATCC 29213). This was achieved by inoculating the bacteria in selective culture media (rapid coliform broth agar for *E. coli* and salted manitol agar for *S. aureus*), followed by 24 h of incubation at 37 °C. After incubation, five colonies of each bacterial species were inoculated into a general culture medium (Muller Hinton+agar broth) and incubated again at 37 °C for another 24 h. After the bacteria colonized their cultivation media, five isolated colonies of each species were selected and transferred to two tubes (one for each species) containing 9 mL of saline solution (8.5 mg/mL of NaCl). The two suspensions were then homogenized in a vortex mixer, and subsequently had their concentration adjusted to 10^8 colony forming units (CFU) per mL, as recommended by the best scientific protocols [28]. The two bacterial suspensions were then further diluted, with liquid Muller Hinton broth, to a concentration of 10^5 CFU/mL. These new 10^5 CFU/mL suspensions were then divided into ten tubes each, and to each were added the following concentrations of Ag/HNT-0 or Ag/HNT-8: 3 ppm, 6 ppm, 12 ppm, 25 ppm, 50 ppm, 100 ppm, 200 ppm, 400 ppm, 800 ppm and 1600 ppm. Finally, each nanoparticle+bacteria suspension was again incubated at 37 °C for 24 h. The minimal inhibitory concentration was determined examining bacterial growth at each nanoparticle concentration.

Dispersion of Ag/HNT-8 in LDPE polymer matrix

Ag/HNT-8 was also tested as an antimicrobial additive to low density polyethylene (LDPE) and the biocide properties of the resulting composite were quantified by means of an antimicrobial surface activity test.

First, two 10 g samples of Ag-NPs were prepared according the process described in the section "silver nanoparticle synthesis". Then, one of the Ag-NP samples was coated with dodecanethiol (DIO) to make its surface hydrophobic and therefore more chemically compatible with LDPE, a

non-polar polymer matrix. This coating was performed suspending the to-be-coated sample in 10 mL of ethanol/dodecanethiol mixture (200:1, v/v) for 24h, followed by filtering, washing with ethanol, and drying at 60 °C for 2h. The coated sample was labelled Ag/HNT-8/DIO, and the DIO coating was considered successful since qualitative tests showed that Ag/HNT-8/DIO did indeed present hydrophobic behaviour, while Ag/HNT-8 did not.

Afterwards, 2 g of Ag/HNT-8 and Ag/HNT-8/DIO were mixed with 650g of LDPE pellets. Both mixtures were homogenized and mould injected into square plates of 8x8cm^2 (95 MPa, 860 mm/s, 1 m double screw, 170 °C injection temperature, 90 °C mold temperature). Polymer plates doped with Ag/HNT-8 and Ag/HNT-8/DIO were characterized by SEM. LDPE plates without any additive were also prepared to be used as control in the antimicrobial test.

Finally, antimicrobial surface activity tests were performed for LDPE samples doped with Ag/HNT-8 and Ag/HNT-8/DIO. The tests were performed following the guidelines specified in the JIS Z2801 standard, and consist in preparing *E. coli* and *S. aureus* suspensions (analogous to the ones produced in the MIC analysis) and exposing them for 24h to the surface of the LDPE plate. Figure 2 shows the experimental layout described above. After incubation, the suspensions are carefully washed away and re-inoculated in the agar cultivation media. The inhibitory activity of the plastic surface was quantified by comparing the number of viable colonies from the suspensions that were exposed to treated LDPE with the number of viable colonies from the suspensions that were exposed to the control polymer.

Results and Discussion

HNT substrates and Ag-NPs characterization

Figure 3 shows the XRD patterns of HNT-8 and Ag/HNT-8 samples. HNT-8 diffraction peaks were fount at 2θ = 11.66°, 20.09° , 23.88°, 35.09° , 37.81°, 54.82° and 62.47°, matching the diffraction planes (001), (100), (002), (110), (003), (210) and (300) of 7Å dehydrated halloysite (JCPDS No. 29-1487); while additional peaks were found at 2θ: 26.57° and 76.80°, matching the diffraction pattern of quartz (JCPDS No. 46-1045), a commonly found secondary phase in HNT samples

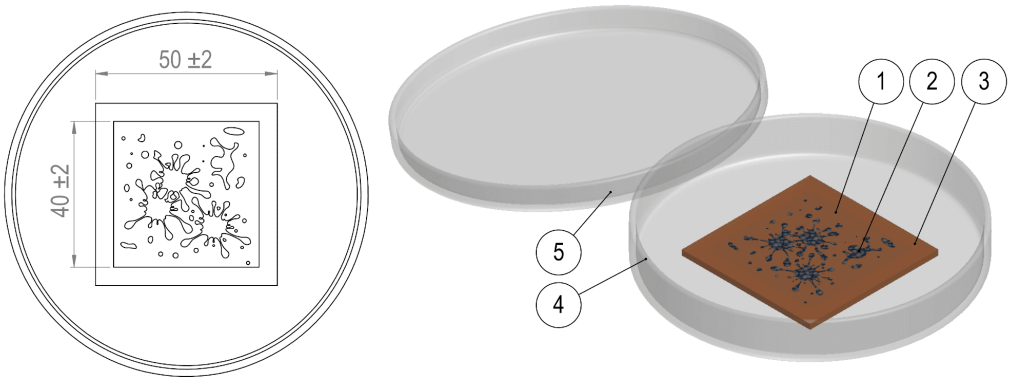

Figure 2: Layout of sample dimensions (in mm x mm) and preparation for the polymer antimicrobial test showing: (1) film cover; (2) bacterial suspension; (3) LDPE test specimen; (4) Petri dish; (5) Petri dish cover.

[29]. This result confirms that the substrate is indeed halloysite clay and the absence of any NaOH phase indicates that the treatment waste was successfully washed away. For Ag/HNT-8 diffraction peaks were found at 2θ: 38.12°, 44.29°, 64.44°, 77.39° and 81.53° matching the planes (111), (200), (220), (311) and (222) of FCC metallic silver (JCPDS No. 04-0783) with a lattice constant of 4.089 Å and estimated crystallite size around of about 40 nm, calculated using Scherrer´s equation:

$$d = 0.9\lambda/B \cdot cos(\theta) \tag{1}$$

where d is the crystallite size, λ is the wavelength of X-ray radiation (0.15418 nm for Cu Kα radiation), B the line width and θ the angle of diffraction for most intense peak, which for the Ag/HNT-8 is (111). These results confirm the formation of well crystallized AgNPs onto the HNT substrates. However only three halloysite peaks were found in Ag/HNT-8, corresponding to: (001), (100) and (002) planes, and their intensity was notably smaller than that of the peaks silver, suggesting no stack of halloysite layers in the composite.

Figure 4 shows TEM images of halloysite substrate samples and of samples that went through silver thermal reduction. HNT-0, HNT-4 and HNT-8 images (figure 4 a, c and e) show that the NaOH treatment induced major structural changes in the HNT substrates. As the treatment progressed,

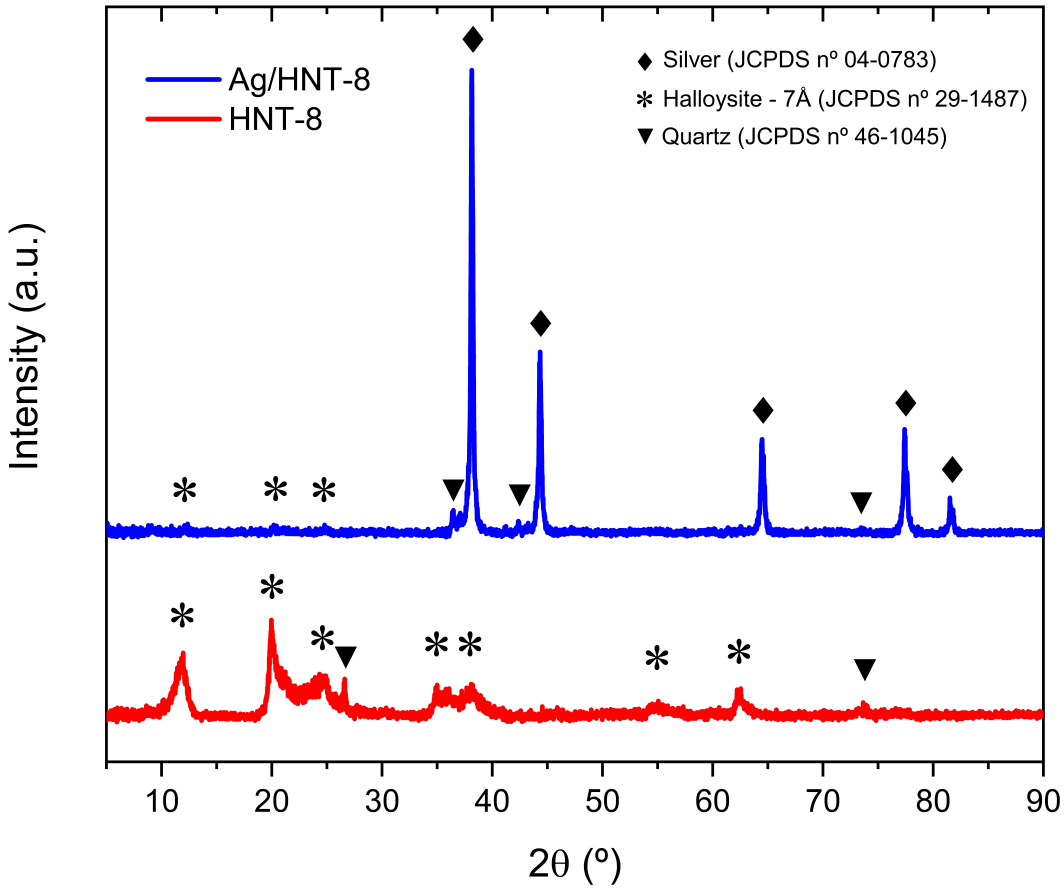

Figure 3: XRD patterns of HNT-8 and Ag/HNT-8.

HNT nanotubes slowly unfolded into nanosheets, starting with the enlargement of HNT's central lumen, as shown in the HNT-4 TEM image (fig. 4C). By day 8, most HNT nanotubes had already turned into nanosheets, as seen in HNT-8 TEM image (fig. 4D). It is known that HNT original nanotubular morphology is a consequence of internal torques into the clay crystalline structure [24]. This torque arises from the fact that while HNT's silicon and aluminol phases share apical oxygen atoms, the oxygen atom's "natural spacing" is different for the two crystalline phases, straining them to conform the oxygen into both structures at the same time. It is our theory that as the NaOH chemical bath etches away Al and Si atoms from HNT [30,31], internal sharing of apical oxygen is reduced, diminishing the internal torque to the point where it is not strong enough to keep the tubular structure anymore.

TEM images for Ag/HNT-0, Ag/HNT-4 and Ag/HNT-8 (figure 4 b, d and f) show the distribution

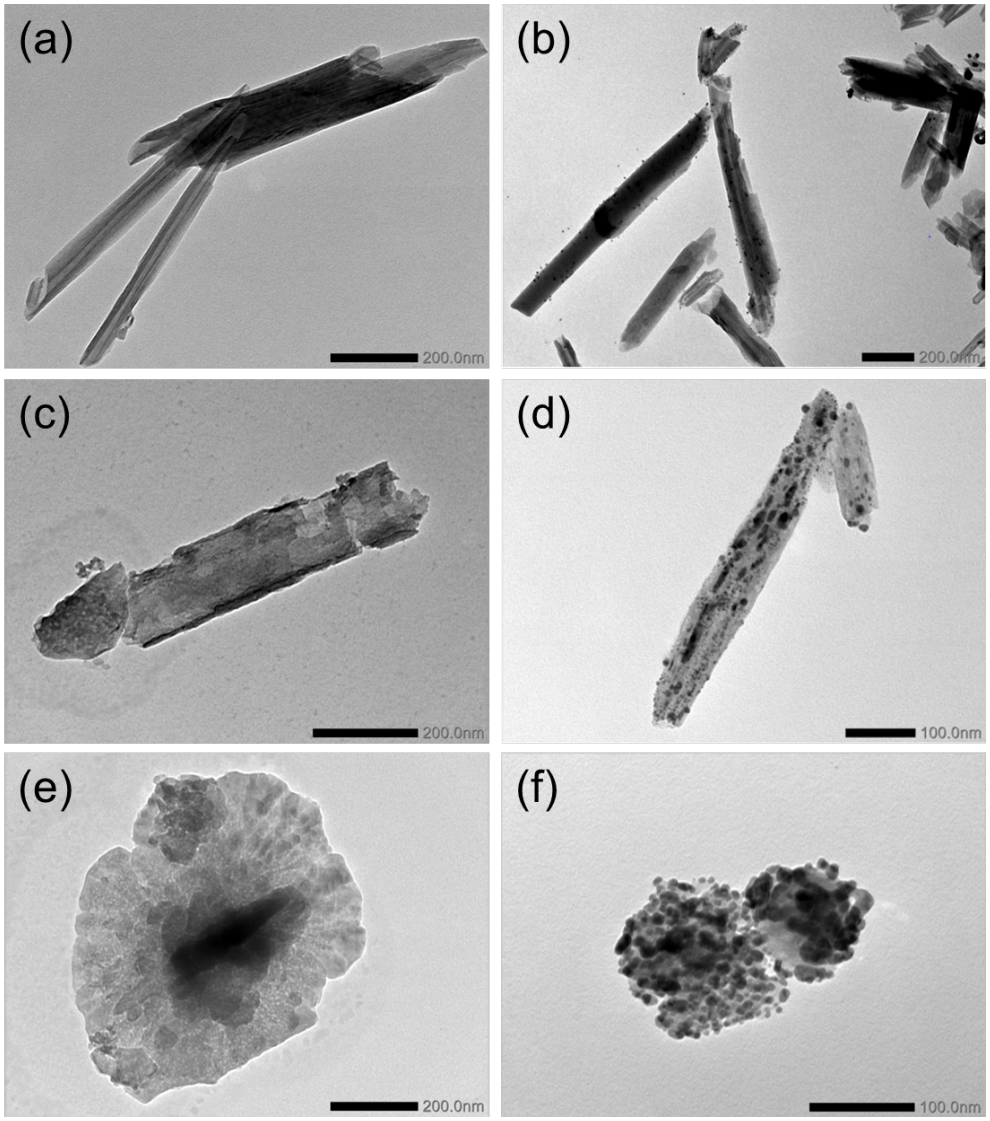

Figure 4: TEM images of: (a) HNT-0; (b) Ag/HNT-0; (c) HNT-4; (d) Ag/HNT-4; (e) HNT-8; (f) Ag/HNT-8.

of metallic silver nanoparticles nucleated onto HNT surface and also show these nucleation increases with treatment time, providing the greater decoration for Ag/HNT-8 sample, as expected. EDS results, presented in table 1, supports this analyses by showing the amount of silver element also increases with treatment time. These results indicates that the NaOH chemical bath indeed improves silver nucleability on HNT clay surface. Three mechanisms can be suggested to explain the improved silver nucleation of samples Ag/HNT-4 and Ag/HNT-8, all of them related to the fact that hydroxyls are preferential nucleating spots for silver:

- *Hydroxilation of HNT's surface*: By exposing the clay particles to NaOH we graft hydroxyls on its surface [32-34], which will later work as nucleating site for Ag-NPs;

- *Inducing crystalline defects by corrosion*: By exposing the HNT clay particles to NaOH(aq), we trigger a corrosion process which slowly etches away the external crystalline phase [30], inducing defects at crystalline structure which expose the internal hydroxyl layer of HNTs to silver nucleation[22];

- *Unfolding of HNT into nanosheets*: Figure 4 shows that as the NaOH treatment proceeded, it made HNT tubes open into sheets, which inevitably exposes the inner aluminol layer (rich in hydroxyls) to silver nucleation.

It is not clear which mechanism is the dominant one. Figure 4(d) and table 1 indicate that Ag/HNT-4 shows improved nucleability even though its substrates did no unfold. This suggests the first mechanism and the second are already significant enough to induced improved nucleability on the clay's surface.

While the original intent of the NaOH bath was to graft hydroxyls into the HNT surface to improve Ag-NPs formation, the opening of the nanotubes into nanosheets was a welcomed surprise, as it exposes the aluminol phase (which is covered by hydroxyls, but originally turned inwards) to silver nucleation.

Table 1: EDS results for Ag-NPs samples (standard deviation between brackets).

Sample	Ag(%)	O(%)	Al(%)	Si(%)
Ag/HNT-0	18.3 (0.4)	49.7 (0.7)	15.6 (0.2)	16.4 (0.2)
Ag/HNT-4	39.8 (2.0)	41.2 (2.1)	9.3 (0.2)	9.7 (0.1)
Ag/HNT-8	46.9 (2.0)	35.2 (1.3)	8.5 (0.1)	9.4 (0.2)

Analysis of silver nanoparticle thermal reduction

The results of HNT's loaded with silver nitrate TGA and DSC analysis are presented in figure 5. Since the sub-products of silver nitrate reduction are oxygen and nitrogen dioxide (both gaseous substances) from reaction: $2AgNO_3 \rightarrow 2Ag_{(s)}+O_2+2NO_{2(g)}$ [35], we expect to see mass reduction

as AgNP nucleates; and since nucleation is an endothermic process, we expect to see endothermic peaks as well. Table 2 compiles such results into five different thermodynamic phases, characterized by different TGA/DSC behaviour. TEM images in figure 5 are meant to correlate the phases described in table 2 with structural changes of the material. Color change during sample heating is presented in figure 6 and also correlated to the data in table 2.

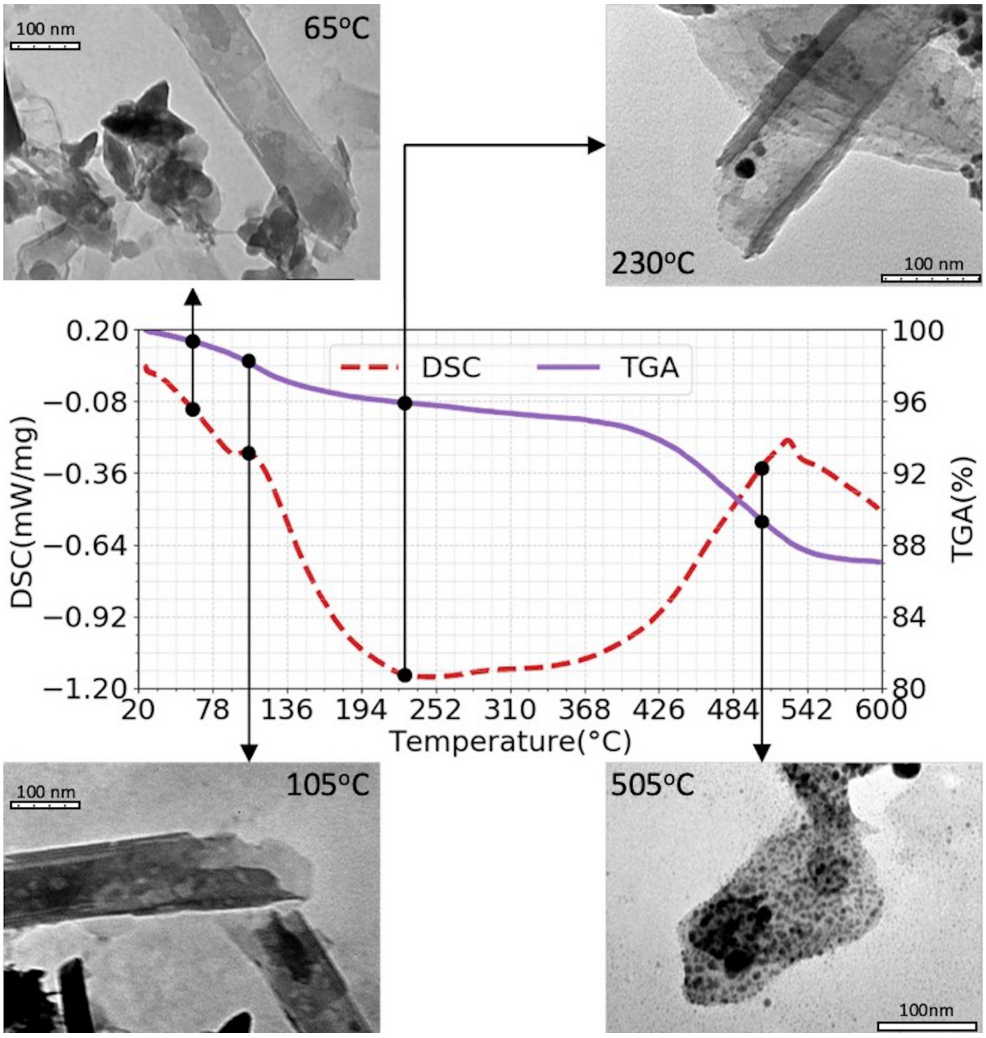

Figure 5: DSC and TGA measurements of Ag-NP formation from room temperature up to 600 °C. TEM image of the samples prepared with the same parameters of the DSC/TGA measurements, but the synthesis was stopped at specific temperatures: 65 °C, 105 °C, 230 °C, 505 °C, to observe the Ag-NP nucleation on the substrates.

At phase I (27 °C - 100 °C) there is a slight mass-loss, which can be attributed to moisture loss, but that does not correspond to any endothermal or exothermal peak. The corresponding TEM image (at 65°C in the inset of fig. 5) shows no formation of Ag-NPs. The lack of NPs suggests that

Table 2: TGA and DSC behaviour by temperature range.

Phase	Range (^{o}C)	TGA Behaviour	DSC Behaviour	Color
I	26 °C - 100 °C	slow rate of mass loss	no event	white
II	100 °C - 135 °C	mass loss at increased rate	endothermal peak	changing to gray
III	135 °C - 420 °C	reduced rate of mass loss	no event	changing to yellow
IV	420 °C - 540 °C	mass loss at increased rate	endothermal peak	brown
V	540 °C - onwards	mass stabilizes (no more losses)	no peak or plato	orange brown

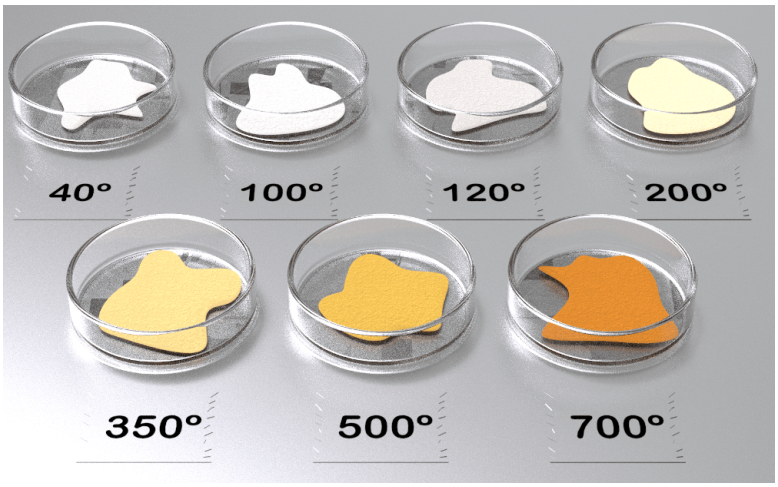

Figure 6: Schematic image of the Ag-NPs with different colors, when the synthesis processes were interrupted at (a) 40 °C, (b) 100 °C, (c) 120 °C, (d) 200 °C, (e) 350 °C, (f) 500 °C, and (g) 700 °C. (In the supplementary material the real image of the nanoparticles powder can be found).

the slight mass loss in the ‘phase I does not indicate any silver nitrate reduction, but only humidity loss. At interval II (100°C - 135°C) the mass-loss increases substantially. The behaviour is concurrent with an endothermal peak. The endothermal behaviour and the fact that the increased rate of mass loss happens near 100 °C (water boiling temperature) strongly suggests that in interval II there is a evaporation process happening on the remaining humidity, left from interval I. Again, the corresponding TEM image (at 105 °C) still shows no Ag-NPs nucleation. At phase III (135 °C - 420 °C) there are no endothermal or exothermal peaks, but there is a low continuous rate of mass-loss, associated with a slight change in the color of the compound, suggesting the beginning of Ag-NPs formation. Indeed, the corresponding TEM image (at 230 °C) shows some Ag-NPs. According to literature, however, silver nitrate is not expected to thermally decompose until 500 °C [35]. An early formation of Ag-NPs suggests that the modified HNT substrate may have some catalytic effect on the $AgNO_3$ decomposition. The low rate of mass loss is consistent with a low rate

of Ag-NP formation. At phase IV (420 °C - 540 °C) there is an increased rate of mass-loss and an endothermal peak, now associated with severe color change, from yellow to brown. This happens near $AgNO_3$'s usual decomposition temperature [35], and suggests acceleration of $AgNO_3$ reduction into metallic silver (when compared to phase III). The corresponding TEM image (at 505 °C) indeed confirms significant presence of Ag-NPs, indicating that phase IV corresponds to most of the nanoparticle's formation. This hypothesis is further strengthened by the fact that in phase V (540 °C - 600 °C) there is no mass loss and no endothermic peak, suggesting that all $AgNO_3$ was already converted into Ag-NPs. Yet, as shown by figure 6, samples heated above 600 °C still presented some colour change. This effect may be due particle growth, which is expected to happen when nanoparticles are heated to higher temperatures.

Antimicrobial Tests

The Minimal Inhibitory Concentration test of AgNP/HNT-8 indicated a MIC of 25 ppm for *E. coli*, and 50 ppm for *S. aureus*, while the MIC of AgNP/HNT-0 was 100 ppm for *E. coli* and 200 ppm for *S. aureus*. The discrepancy between antimicrobial effect against *E. coli* and *S. aureus* can be explained by morphological differences between the two bacteria. Being a gram-positive bacteria, *S. aureus* has a thicker cell wall than *E. coli*, and thus the silver ions responsible to kill them have a harder time penetrating into the cell's core. This result in consistent with the expected antimicrobial effects of Ag-NPs. Results indicate that AgNP/HNT-8 has a stronger antimicrobial effect than AgNP/HNT-0, which can be explained by the higher silver content of AgNP/HNT-8.

The JIS Z 2801 antimicrobial surface activity test shows that 19.64% of *E. coli* colonies and 96.02% of *S. aureus* colonies were able to proliferate into LDPE doped with Ag/HNT-8; while the LDPE doped with Ag/HNT-8/DIO showed no signs of proliferation at all, indicating a dramatic increase in antimicrobial activity. Figure 7 shows SEM images of both plastic samples, and shed light on why Ag/HNT-8/DIO was able to better transfer its antimicrobial properties to LDPE. The uncoated sample (figure 7a) displays the formation of microscopic clusters, which are associated to Ag-NPs aggregates; in contrast the Ag/HNT-8/DIO doped sample (figure 7b) shows a relatively

smooth surface, displaying fewer particle clusters and far more nanoscaled dots, suggesting a better dispersion of coated particles into the LDPE matrix. As the antimicrobial properties of Ag-NPs are associated with the release of Ag^+ ions [36], and as this release is correlated with the surface energy of nanoparticles. Thus, the higher antimicrobial surface activity obtained with Ag/HNT-8/DIO is consistent with expectations, as well dispersed nanoparticles tend to have higher surface energy.

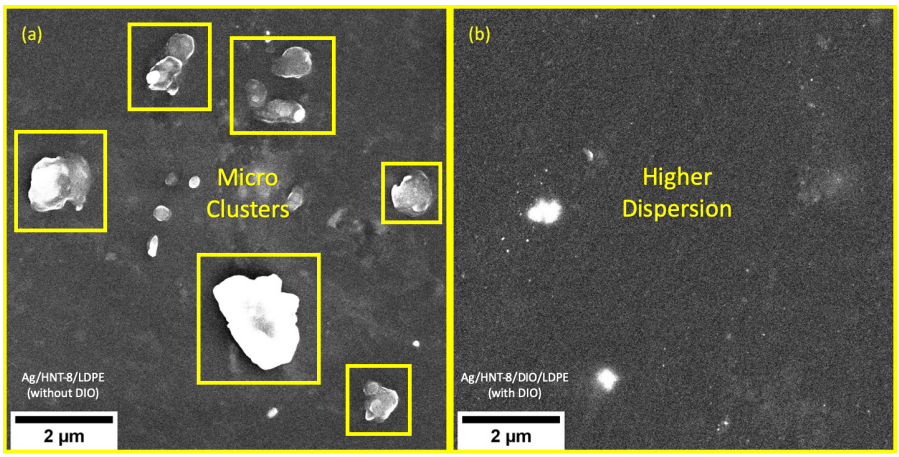

Figure 7: Scanning electron microscopy of Ag/HNT-8 doped LDPE (a), and Ag/HNT-8/DIO doped LDPE (b).

The difference in aggregation between both samples may be explained in terms of matrix polarity. Polymer molecules are polarized to some degree, depending on the type of material. Polyethylene (both low and high density) is almost apolar, and thus mix very well with hydrophobic particles and very bad with hydrophilic ones. Qualitative tests have shown that while Ag/HNT-8 gets wet in water, Ag/HNT-8/DIO is highly hydrophobic. This hydrophobic behaviour is most certainly due to the presence of DIO – a very hydrophobic substance itself. DIO is an organic molecule made from a long carbon chain "tail" attached to a thiol "head" (R-SH), which happens to form covalent bonds with silver in virtue of it's sulfur atom. So, by mixing DIO and Ag/HNT-8 one is able to create a thin layer of carbonic chains going out of Ag/HNT-8's surface (as shown in figure 8), imbuing them with hydrophobic properties, which results in better dispersability into the LDPE matrix and consequently in better antimicrobial surface activity for plastics doped with the coated sample.

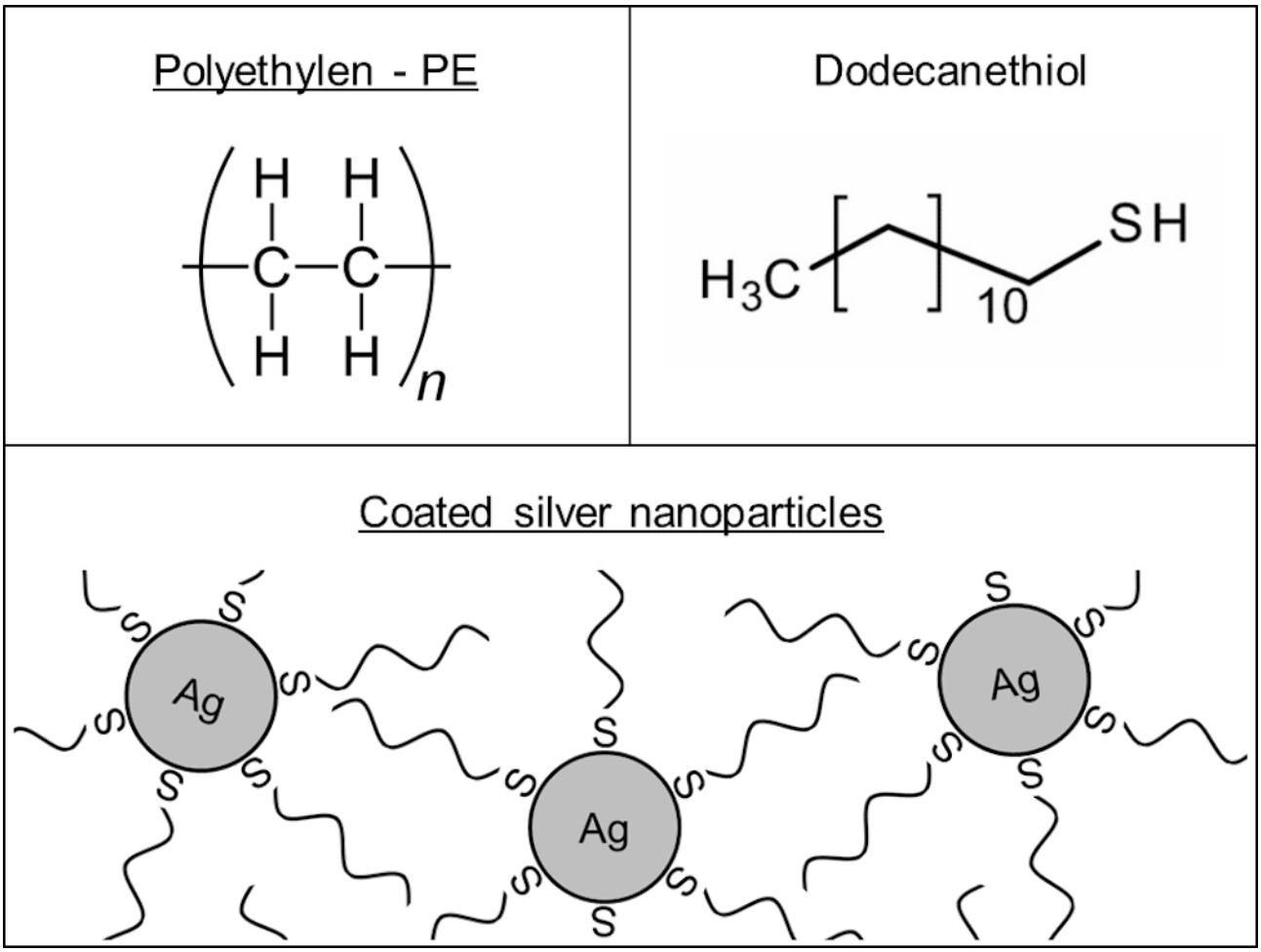

Figure 8: Molecular structure of polyethylene (PE), molecular structure of dodecanethiol (DIO), and scheme for Ag-NPs coated with dodecanethiol.

Conclusion

Treating halloysite with NaOH is an efficient way to enhance silver nucleation into the clay's surface. Substrates treated with this technique were able to anchor the formation of nanosized silver particles, that displayed strong antimicrobial effect against *E. coli* and *S. aureus*, as was expected. The resulting antimicrobial effect for treated substrates was also higher than for the untreated halloysite. TGA and DSC analysis indicated that most reduction of metallic silver from $AgNO_3$ into halloysite substrates occurs at temperatures above 420 ^{o}C, while TEM images showed that nucleation at this temperature does not result in uncontrolled grain growth into microscopic scale. The Ag-NPs produced in this work were also tested for practical applications by dispersing them into

LDPE matrices and measuring the resulting composite's surface antimicrobial activity. While the antimicrobial effect of LDPE doped with "natural" Ag-NPs was disappointing, it was possible to greatly improve the material's antimicrobial properties by coating the nanoparticles with dodecanethiol – a non-polar surfactant agent, highly compatible with LDPE. This shows that the Ag-NPs synthetized is this work are viable as antimicrobial additives for plastics — probably the most important material for large scale industrial applications — while also highlighting the importance of controlling chemical affinity between nanoparticle's surface and matrix, a fact often overlooked in nanoparticle's literature.

The synthesis process presented in this work uses only common reactants, thermal reduction and the inexpensive halloysite clay as substrate, being thus a low cost solution for antimicrobial nanoparticle production, that is also scalable to industrial production.

Acknowledgements

We acknowledge CNPq, CAPES, FAPEMIG and Fundação Araucária for funding part of this work. We also acknowledge nanotropic ltda. for supporting our work.

References

1. Scheres, J.; Kuszewski, K. *Zeszyty Naukowe Ochrony Zdrowia. Zdrowie Publiczne i Zarzadzanie* **2019**, *17* (1), 2–8.

2. Wang, Y.; Yang, Y.; Shi, Y.; Song, H.; Yu, C. *Advanced Materials* **2020**, *32* (18), 1904106.

3. Wang, L.; Hu, C.; Shao, L. *International journal of nanomedicine* **2017**, *12*, 1227.

4. Cheeseman, S.; Christofferson, A. J.; Kariuki, R.; Cozzolino, D.; Daeneke, T.; Crawford, R. J.; Truong, V. K.; Chapman, J.; Elbourne, A. *Advanced Science* **2020**, *7* (10), 1902913.

5. Slavin, Y. N.; Asnis, J.; Häfeli, U. O.; Bach, H. *Journal of nanobiotechnology* **2017**, *15* (1), 1–20.

6. Kaushik, M.; Niranjan, R.; Thangam, R.; Madhan, B.; Pandiyarasan, V.; Ramachandran, C.; Oh, D.-H.; Venkatasubbu, G. D. *Applied Surface Science* **2019**, *479*, 1169–1177.

7. Dizaj, S. M.; Lotfipour, F.; Barzegar-Jalali, M.; Zarrintan, M. H.; Adibkia, K. *Materials Science and Engineering: C* **2014**, *44*, 278–284.

8. Gharpure, S.; Akash, A.; Ankamwar, B. *Journal of nanoscience and nanotechnology* **2020**, *20* (6), 3303–3339.

9. Huang, Y.; Mei, L.; Chen, X.; Wang, Q. *Nanomaterials* **2018**, *8* (10), 830.

10. Sondi, I.; Salopek-Sondi, B. *Journal of colloid and interface science* **2004**, *275* (1), 177–182.

11. Kim, J. S.; Kuk, E.; Yu, K. N.; Kim, J.-H.; Park, S. J.; Lee, H. J.; Kim, S. H.; Park, Y. K.; Park, Y. H.; Hwang, C.-Y. et al. *Nanomedicine: Nanotechnology, Biology and Medicine* **2007**, *3* (1), 95–101.

12. Pinzaru, I.; Coricovac, D.; Dehelean, C.; Moacă, E.-A.; Mioc, M.; Baderca, F.; Sizemore, I.; Brittle, S.; Marti, D.; Calina, C. D. et al. *Food and Chemical Toxicology* **2018**, *111*, 546–556.

13. Kaur, A.; Kumar, R. *RSC advances* **2019**, *9* (2), 1095–1105.

14. Stavitskaya, A.; Batasheva, S.; Vinokurov, V.; Fakhrullina, G.; Sangarov, V.; Lvov, Y.; Fakhrullin, R. *Nanomaterials* **2019**, *9* (5), 708.

15. Yuan, Q.; Golden, T. D. *Surfaces and Interfaces* **2020**, *20*, 100620.

16. Burridge, K.; Johnston, J.; Borrmann, T. *Journal of Materials Chemistry* **2011**, *21* (3), 734–742.

17. Maisanaba, S.; Pichardo, S.; Puerto, M.; Gutiérrez-Praena, D.; Cameán, A. M.; Jos, A. *Environmental research* **2015**, *138*, 233–254.

18. Tokarskỳ, J.; Čapková, P.; Rafaja, D.; Klemm, V.; Valášková, M.; Kukutschová, J.; Tomášek, V. *Applied surface science* **2010**, *256* (9), 2841–2848.

19. Ge, M.; Li, J.; Song, S.; Meng, N.; Zhou, N. *Applied Clay Science* **2019**, *183*, 105334.

20. Praus, P.; Turicová, M.; Machovič, V.; Študentová, S.; Klementová, M. *Applied clay science* **2010**, *49* (3), 341–345.

21. Zhang, Y.; Chen, Y.; Zhang, H.; Zhang, B.; Liu, J. *Journal of inorganic biochemistry* **2013**, *118*, 59–64.

22. Abdullayev, E.; Sakakibara, K.; Okamoto, K.; Wei, W.; Ariga, K.; Lvov, Y. *ACS applied materials & interfaces* **2011**, *3* (10), 4040–4046.

23. Liu, P.; Zhao, M. *Applied Surface Science* **2009**, *255* (7), 3989–3993.

24. Singh, B. *Clays and Clay Minerals* **1996**, *44* (2), 191–196.

25. Musino, D.; Rivard, C.; Landrot, G.; Novales, B.; Rabilloud, T.; Capron, I. *Journal of Colloid and Interface Science* **2020**, *584*, 360–371.

26. Jana, S.; Kondakova, A. V.; Shevchenko, S. N.; Sheval, E. V.; Gonchar, K. A.; Timoshenko, V. Y.; Vasiliev, A. N. *Colloids and Surfaces B: Biointerfaces* **2017**, *151*, 249–254.

27. Lvov, Y.; Wang, W.; Zhang, L.; Fakhrullin, R. *Advanced Materials* **2016**, *28* (6), 1227–1250.

28. Wiegand, I.; Hilpert, K.; Hancock, R. E. *Nature protocols* **2008**, *3* (2), 163.

29. Daou, I.; Lecomte-Nana, G. L.; Tessier-Doyen, N.; Peyratout, C.; Gonon, M. F.; Guinebretiere, R. *Minerals* **2020**, *10* (5), 480.

30. Langston, R.; Jenne, E. *Clays and Clay Minerals* **1963**, *12* (1), 633–647.

31. White, R. D.; Bavykin, D. V.; Walsh, F. C. *Nanotechnology* **2012**, *23* (6), 065705.

32. D'Souza, A. S.; Pantano, C. G. *Journal of the American Ceramic Society* **2002**, *85* (6), 1499–1504.

33. Dupuis, R.; Pellenq, R.; Champenois, J.-B.; Poulesquen, A. *The Journal of Physical Chemistry C* **2020**, *124* (15), 8288–8294.

34. Zeng, S.; Reyes, C.; Liu, J.; Rodgers, P. A.; Wentworth, S. H.; Sun, L. *Polymer* **2014**, *55* (25), 6519–6528.

35. Stern, K. H. *Journal of Physical and Chemical Reference Data* **1972**, *1* (3), 747–772.

36. Feng, Q. L.; Wu, J.; Chen, G. Q.; Cui, F.; Kim, T.; Kim, J. *Journal of biomedical materials research* **2000**, *52* (4), 662–668.